Modal Theory of Phase-Modulated and Frequency-Shifting Ring Cavities

MIGUEL CUENCA*, HAROLDO MAESTRE, AND CARLOS R. FERNÁNDEZ-POUSA

Engineering Research Institute I3E, Univ. Miguel Hernández, Av. Universidad s/n, 03202 Elche, Spain
*miguel.cuenca02@goumh.umh.es

Abstract: A theoretical and experimental characterization of the optical modes of dispersionless ring cavities incorporating phase modulators (PM) and/or frequency shifters (FS) is presented. Using linear operator theory, the exact response of these cavities to arbitrary modulating waveforms and optical inputs is computed and shown to be a filtering process that selects a certain class of fields, invariant under multiple roundtrips, which are identified with the cavity's optical modes. The different types of PM/FS cavity modes are analyzed. This approach also leads to a representation of these cavities as unmodulated resonators preceded and followed by complementary phase modulations, which are linearly related to the imparted intracavity phase modulation or frequency shift. The theory is experimentally validated by the external injection of engineered phase and frequency modulated cavity modes in an Er:fiber PM fiber loop, and also compared with the emission modes of FM lasers and CW frequency-shifted feedback lasers. These results provide a unified view for the linear analysis of systems employing PM/FS active cavities or resonators, of interest in the field of photonic signal generation and processing.

1. Introduction

An ample variety of optical systems uses as a key building block an optical resonator or active cavity incorporating a phase modulator or a frequency shifter. Leveraging the large modulation bandwidth attainable after multiple recirculations, optical frequency combs have been generated in active phase-modulated (PM) fiber loops [1–4], resonant phase modulators [5–8] and integrated PM ring resonators [9–15]. Recirculating PM fiber loops or ring resonators have also been used as photonic analogs of numerous dynamical systems, such as kicked rotors [16] and random walks or Bloch oscillations modeled as tight-binding hamiltonians in the synthetic dimension of frequency [17–23]. In the time domain, amplified PM and frequency-shifting (FS) fiber loops are actively explored as wideband photonic signal generators and processors [24–30].

In a different context, the incorporation of frequency shifters and phase modulators in an active cavity has long been known to result in particular types of laser emission. In the case of phase modulators, when the driving frequency is tuned to the cavity's free spectral range (FSR) or to one of its harmonics, the resulting FM-modelocked emission sets in the form of chirped pulses. When the driving departs from the tuned frequency, typically at relative values below the 1%, the emission is no longer pulsed but of constant amplitude. In this, so called, FM laser regime, the emission features a wide sinusoidal instantaneous frequency which broadens the optical spectrum in a distribution that follows the Bessel functions [31, 32]. If, in turn, a frequency shifting device is placed inside the laser cavity, the emission of the resulting frequency-shifted feedback (FSF) laser appears devoid of spectral structure [33, 34]. The output is understood as composed of linearly chirped waves that are continuously generated from ASE and regeneratively amplified as they shift in frequency through the spectral net gain region. Such a description is referred to as the moving comb model of CW FSF laser emission [35–39]. With increasing pump powers, lasers of this type also show Q-switched and modelocked regimes [40, 41].

The description of these systems usually relies on the concrete type of application. In PM loops and cavities, the response is described as a series of delayed and phase-modulated replicas of the input [1, 25]. The frequency domain, in turn, is best suited to the analysis of synthetic dynamical systems [20, 21]. FM lasers were initially described in the frequency domain through coupled-mode equations [31, 32]. In the time domain, they have been described using Haus' master equation [42] and also the Maxwell-Bloch equations subject to a periodic phase perturbation, either numerically [43] or through Floquet analysis [44]. In these descriptions, exact solutions are scarce, with some exception such as the modal solution of FM lasers [31, 32, 42].

In this paper, we address the linear analysis of optical ring cavities incorporating phase modulation and/or frequency shifting. This exploration is motivated, on the one hand, by the wide variety of photonic processors incorporating PM/FS cavities that would benefit from a compact description at system's level and, on the other, by the quest of optical generators of user-defined, reconfigurable optical waveforms. Our approach relies on the observation that, for both passive and active PM/FS ring cavities operated below threshold, the recirculation process can be considered devoid of nonlinear propagation and gain saturation effects. If, in addition, the cavity is dispersionless, the linear recirculation admits an exact solution that accounts for arbitrary inputs and arbitrary phase modulation profiles or frequency shifting. The theory is solved in Section 2 in operator formalism, which is a convenient tool for the identification of the PM/FS cavity modes from the complete set of eigenfunctions. These modes are phase-modulated fields carried by the axial modes of the unmodulated resonator, invariant under multiple roundtrips and of minimum bandwidth. In that section we also analyze the different families of cavity modes that can be generated. This approach leads to an alternative representation of PM/FS cavities as unmodulated resonators sandwiched by complementary phase modulations, linearly related by a recursive formula to the imparted intracavity phase modulation or frequency shift and coincident with the modal phase of the PM/FS cavity mode. In Section 3, we experimentally validate the theory in a PM Er:fiber loop through the external injection of different PM cavity modes. We also present the characterization of single and multimode FM and CW FSF laser emission and its relationship with the cavity modes using digital correlation techniques, analyzing the limitations of standard spectrotemporal characterization tools for the modal analysis of these lasers. Finally, we end in Section 4 with our conclusions. Preliminary results were presented in [45].

Particular forms of our results have been described in the rich literature of PM/FS cavities and FM/FSF lasers. An operator theory of PM cavities was developed in [46] for the analysis of the broadband light generated by sinusoidal phase modulation, of which the present theory represents the exact solution in the dispersionless limit. The recursive formula (7) that defines the modal phase was used in studies of electro-optical tunable microchip FM lasers [43], of SOA-based fiber FM lasers [47] and, more recently, of electro-optically phase modulated ring resonators [48]. A similar recursive relationships, but defined in frequency, was employed [49] to describe the operational principle of FM lasers. In [48] it was also introduced an equivalent representation of the PM resonator that is here generalized to PM/FS cavities. Self-consistency arguments, equivalent to our definition of cavity modes, were also used in [49], and in [35], for the determination of FM and FSF laser emission modes, respectively. Our results unify these descriptions in a common framework that applies to FS and PM cavities, or combination of both, providing a deeper understanding of their response to general input waves and complementing the different approaches used in the analysis of the corresponding laser emission.

2. Theory

Let us consider the recirculation of an optical field in a dispersionless ring cavity or resonator with roundtrip time τ_c and FSR $\omega_c = 2\pi/\tau_c$ in a single spatial mode, where it recursively undergoes phase modulation or frequency shifting. The modulation is assumed lumped and described by a multiplying term $\exp(j\varphi(t))$. In the case of PM cavities, $\varphi(t) = \pi V(t)/V_\pi$ where $V(t)$ is the driving voltage and V_π the modulator's half-wave voltage. As any dc bias in the driving voltage can be absorbed in the definition of τ_c we may assume that $\varphi(t)$ is dc-free. In the case of FS cavities, $\varphi(t) = \Omega_s t$ where Ω_s is the shifting frequency.

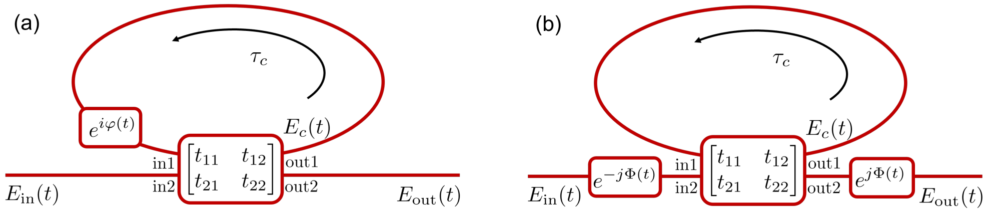

Fig. 1. (a) Scheme of a phase modulated resonator. (b) Equivalent representation.

As is shown in Fig. 1(a), which follows the notation of [25], optical fields $E_{\text{in}}(t)$ and $E_{\text{out}}(t)$ are respectively injected and extracted from the resonator through a linear 2×2 passive network described by a transmission matrix with entries t_{ij} $(i, j = 1, 2)$. The intracavity field, referred to the network's output (out1), is denoted by $E_c(t)$ so that the corresponding input (in1) is $\overline{\rho} e^{j\varphi(t)} E_c(t - \tau_c)$ with τ_c the roundtrip time and $\overline{\rho} < 1$ the roundtrip amplitude decay factor, excluding the injection/extraction network loss. Then, the network equations are:

$$
\begin{aligned}
E_c(t) &= t_{11}\overline{\rho} e^{j\varphi(t)} E_c(t - \tau_c) + t_{12} E_{\text{in}}(t) \\
E_{\text{out}}(t) &= t_{21}\overline{\rho} e^{j\varphi(t)} E_c(t - \tau_c) + t_{22} E_{\text{in}}(t)
\end{aligned} \tag{1}
$$

The first of these equations represents a boundary condition for the intracavity field, which will be presented as:

$$
E_c(t) = \rho e^{j\varphi(t)} E_c(t - \tau_c) + E_s(t) \tag{2}
$$

with $\rho = t_{11}\overline{\rho} < 1$ the total roundtrip amplitude attenuation factor and $E_s(t) = t_{12} E_{\text{in}}(t)$ the seed field. The second equation in (1) gives the output $E_{\text{out}}(t)$ in terms of the input $E_{\text{in}}(t)$, the intracavity field $E_c(t)$, and the characteristics of the injection/extraction network. The problem is reduced to the analysis of (2), which represents a linear, time-variant system with input $E_s(t)$ and output $E_c(t)$.

Let us define the unitary operator $U = e^{i\varphi(t)} T$ composition of the intracavity phase modulation and the time translation by the cavity's roundtrip time, $TE(t) = E(t - \tau_c)$. Then, (2) writes $(I - \rho U) E_c(t) = E_s(t)$, with I the identity operator. The solution to this equation can be written as a Neumann series:

$$
E_c(t) = (I - \rho U)^{-1} E_s(t) = \sum_{n=0}^{\infty} \rho^n U^n E_s(t) \tag{3}
$$

which is convergent for $\rho < 1$ since U is unitary. We now compute the eigenfunctions of unitary U, with phase eigenvalues denoted for convenience in terms of an arbitrary frequency ω as $e^{-j\omega\tau_c}$. The eigenvalue equation writes:

$$
e^{j\varphi(t)} E_\omega(t - \tau_c) = e^{-j\omega\tau_c} E_\omega(t) \tag{4}
$$

To solve this functional equation we first notice that the amplitude of $E_\omega(t)$ is periodic with period τ_c. Moreover, the multiplication of any solution of (4) by a periodic phase term is also a solution. This implies that $E_\omega(t)$ is the product of an arbitrary periodic complex field $E_p(t) = E_p(t + \tau_c)$ times an unknown phase term, denoted as $e^{j\Phi(t) + j\omega t}$, and so the form of the eigenfunctions is:

$$
E_\omega(t) = e^{j\Phi(t) + j\omega t} E_p(t) \tag{5}
$$

Substitution of this ansatz in (4) requires that $\Phi(t)$ verifies

$$
\Phi(t) = \Phi(t - \tau_c) + \varphi(t) + 2\pi n \tag{6}
$$

with n integer. Nonetheless, and without loss of generality, function $\Phi(t)$ can be determined as:

$$\Phi(t) = \Phi(t - \tau_c) + \varphi(t) \tag{7}$$

a linear recursion that represents a finite-time integrator. Indeed, a solution $\Phi(t)$ of (7) gives rise to a solution $\overline{\Phi}(t) = \Phi(t) - n\omega_c t$ of (6) and conversely. The additional phase term $e^{-jn\omega_c t}$ is periodic with period τ_c and can be absorbed in $E_p(t)$. For the same reason, we exclude additive periodic terms from the admissible solutions of (7). These mathematical constraints lead to an unambiguous definition of optical modes, as will be explained below. Without reference to these constraints, (7) has been introduced as a means to solve (2) in [47, 48].

Equation (7) also implies that $U = e^{j\varphi(t)}T$ is unitarily equivalent to the temporal translation, $U = e^{j\varphi(t)}T = e^{j\Phi(t)}Te^{-j\Phi(t)}$, and therefore solution (3) can be written as

$$E_c(t) = e^{j\Phi(t)}(I - \rho T)^{-1}e^{-j\Phi(t)}E_s(t) \tag{8}$$

The resolvent operator is diagonal in the Fourier basis, where $T = e^{-j\omega\tau_c}$ with ω the optical frequency:

$$(1 - \rho T)^{-1} = \frac{1}{1 - \rho e^{-j\omega\tau_c}} \equiv H_R(\omega) \tag{9}$$

In this formula, we have defined the optical transfer function of the unmodulated ring resonator $H_R(\omega)$, which represents its filtering characteristics as resonances centered at equispaced optical frequencies multiples of the cavity's FSR. Changing to the Fourier domain to describe the response of the unmodulated ring, the general solution (8) can be explicitly written in terms of the seed as:

$$E_c(t) = \iint \frac{d\omega}{2\pi} dt' \frac{e^{j\omega(t-t')+j(\Phi(t)-\Phi(t'))}}{1 - \rho e^{-j\omega\tau_c}} E_s(t') \tag{10}$$

Also, solution (8) can be transferred to in/out fields using the second equation in (1):

$$E_{\text{out}}(t) = e^{j\Phi(t)} \left[\frac{t_{21}t_{12}}{t_{11}} \frac{\rho T}{1 - \rho T} + t_{22} \right] e^{-j\Phi(t)} E_{\text{in}}(t) \tag{11}$$

The term in brackets represents the filtering properties of an unmodulated ring resonator with an injection/extraction network t_{ij}. Thus, (11) shows that the PM/FS cavity is equivalent to an unmodulated cavity preceded and followed by complementary modulations $\exp(\pm j\Phi(t))$, which are responsible for a unitary change in the field's description. This implies that the system can be represented in a form where modulation and cavity act independently [48], as is schematically shown in Fig. 1(b).

It can be straightforwardly shown that the eigenfunctions (5) are also eigenfunctions of the linear system (8) with eigenvalue $H_R(\omega)$: if a PM/FS cavity is seeded with $E_\omega(t)$, its intracavity field $E_c(t)$ equals the seed field times factor $H_R(\omega)$. By analogy with a standard ring cavity or resonator, we can ascribe the modal content of the PM/FS resonator to those fields with maximum transmission or, equivalently, with maximum eigenvalue $\max|H_R(\omega)| = (1 - \rho)^{-1}$ [46]. These modes are waves phase-modulated by $\Phi(t)$ and carried by the axial modes of the unmodulated resonator. A convenient description of the modal content of a high-Q PM/FS resonator is thus:

$$E_m(t) = e^{j\Phi(t)}E_p(t) = e^{j\Phi(t)} \sum_k A_k e^{jk\omega_c t} \tag{12}$$

with A_k arbitrary complex constants. For this reason, $\Phi(t)$ will be referred to as the *modal* phase function. Again in analogy with an unmodulated ring resonator, these modes can also be determined as those eigenfunctions with eigenvalue one, or simply fields invariant under a lossless roundtrip, $e^{j\varphi(t)}E_m(t-\tau_c) = E_m(t)$. Now we can clarify the constraints imposed during the derivation of (7): a phase term $e^{-jn\omega_c t}$ added to $e^{j\Phi(t)}$ in (12) simply shifts the modal index k, and a resonant phase term, namely periodic with period τ_c, represents a redefinition in the modal amplitudes of the unmodulated resonator. Indeed, using the Fourier series $\exp(j\Phi_p(t)) = \sum_n C_n \exp(jn\omega_c t)$ in the sum of (12) we find:

$$e^{j\Phi_p(t)} \sum_k A_k e^{jk\omega_c t} = \sum_{k,n} C_n A_{k-n} e^{jk\omega_c t} \equiv \sum_k B_k e^{jk\omega_c t} \tag{13}$$

In both cases no generality is gained as compared with (12). The modes of the PM/FS cavity are thus the fields $A_k e^{j\Phi(t)+jk\omega_c t}$ with k positive integer and $\Phi(t)$ given by (7) and free of additive resonant terms. In physical terms, this means that the modes are phase modulated waves of minimum bandwidth carried by the axial modes of the unmodulated resonator, as the multiplication by any resonant phase modulation term $\exp(j\Phi_p(t))$ would always increase the modal bandwidth. This definition is consistent with the modes of unmodulated resonators, which are recovered when $\varphi(t)$, and thus $\Phi(t)$, vanishes.

The phase modulation $\Phi(t)$ that precedes and comes after the unmodulated resonator in the equivalent model of Fig. 1(b) coincides with the modal phase. Due to the linearity of (7), if the intracavity PM/FS modulation is composed of several additive terms, say $\varphi(t) = \varphi_1(t) + \varphi_2(t)$, one can choose equivalent representations where only a part of $\varphi(t)$, say $\varphi_1(t)$, is extracted from the loop through the corresponding (partial) modal phase $\Phi_1(t)$. We also note that, after taking the derivative, we can present (7) in terms of the instantaneous modal frequency $\omega_i(t) = d\Phi/dt$ as [49]:

$$\omega_i(t) = \omega_i(t-\tau_c) + \frac{d\varphi}{dt} \tag{14}$$

indicating that $\omega_i(t)$ is increased in each roundtrip by the Doppler frequency shift imparted by the intracavity modulator. Due to the similarity with (7), the analysis of PM/FS cavities from the perspective of frequency modulation is thus similar. We now proceed to compute and analyze the solutions of (7) for the concrete cases of PM and FS cavities. In the Appendix, we present an additional property of (7) that allows for the extension of the range of available solutions to modulation function incorporating resonant modulations.

2.1. Phase-modulated cavities

The modal phase function of a PM cavity can be derived from (7) using Fourier theory. We denote by $\widehat{\varphi}(\Omega_m)$ and $\widehat{\Phi}(\Omega_m)$ the Fourier transforms of $\varphi(t)$ and $\Phi(t)$, respectively, where the modulation frequency is denoted by Ω_m. Then, (7) can be solved in terms of a modulation transfer function [48],

$$H_{\mathrm{M}}(\Omega_m) = \frac{\widehat{\Phi}(\Omega_m)}{\widehat{\varphi}(\Omega_m)} = \frac{1}{1-e^{-j\Omega_m\tau_c}} \tag{15}$$

provided that Ω_m is off-resonance ($\Omega_m\tau_c/2\pi$ not integer). In the simplest example of sinusoidal phase modulation, the phase function is $\varphi(t) = \mu\cos(\Omega_m t + \theta)$ with μ the modulation index and θ a constant phase. The solution to (7) writes:

$$\Phi(t) = \beta \sin(\Omega_m(t + \tau_c/2) + \theta) \tag{16}$$

with a modulation index given by:

$$\beta = \frac{\mu}{2\sin(\frac{1}{2}\Omega_m\tau_c)} \tag{17}$$

It is illustrative to compare this result with the oscillation modes of an FM laser as [31, 32, 42] or with the broadband light generated in a sinusoidal PM cavity as described in [46]. In these cases,

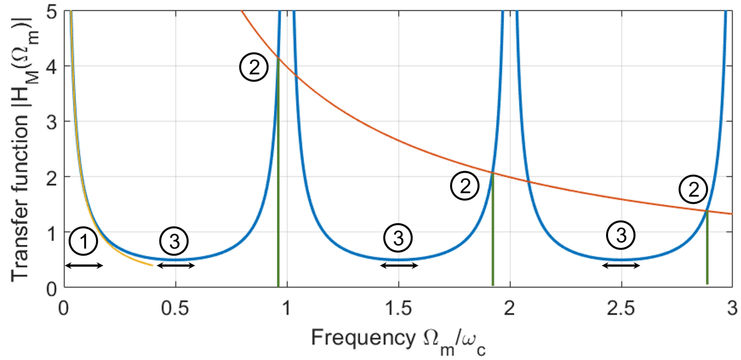

Fig. 2. Blue: amplitude of the modulation transfer function $H_M(\Omega_m)$. Yellow: approximation near dc as an integrator with time constant τ_c. Orange: amplitude of the transfer function of an integrator with time constant $\Delta\tau \ll \tau_c$. Green: spectral lines of a waveform with a frequency close to the FSR. The circled numbers refer to the different regimes explained in the text.

the phase modulator is driven by a sinusoidal waveform at a frequency Ω_m close to the cavity's FSR ω_c or to one of its harmonics,

$$\Omega_m = k\omega_c \pm \Delta\Omega_m \tag{18}$$

with k positive integer and $0 < \Delta\Omega_m \ll \omega_c$. In the present formalism, the PM cavity modes are sinusoidal phase-modulated fields given by (16) which, in the limit $\Delta\Omega \ll \omega_c$, are:

$$\Phi(t) \simeq \pm\frac{\mu}{\Delta\Omega_m\tau_c}\sin(\Omega_m t + \theta) \tag{19}$$

in agreement with the form of FM laser modes and sinusoidal broadband light. The generality of the present approach is apparent as it extends the modal concept to general off-resonance phase modulations of arbitrary functional form. In this regard, several families of modes can be identified in different regimes of the transfer function $H_\mathrm{M}(\Omega_m)$, which we describe next in separate paragraphs.

• Referring to Fig. 2, if the bandwidth of the input phase function $\varphi(t)$ is $\ll \omega_c$, and thus its spectral content is contained in region 1, the transfer function behaves as $H_\mathrm{M}(\Omega_m) \simeq 1/j\Omega_m\tau_c$ and represents an integrator with time constant $1/\tau_c$. This approximation is plotted with a yellow line in Fig. 2. In this region, (7) can be approximated as

$$\tau_c\frac{d\Phi}{dt} = \varphi(t) \tag{20}$$

and so the modal phase has an instantaneous frequency that follows the shape of the imparted phase function.

• If the imparted phase function $\varphi(t)$ is periodic with a fundamental frequency Ω_m close to the FSR or to one of its harmonics, as given by (18), then the spectral content of $\varphi(t)$ consists of frequencies $k\Omega_m$ with $k = \pm 1, \cdots \pm N$ integers, depicted in Fig. 2 as green spectral lines marked with 2. Assume also that $N\Delta\Omega_m \ll \omega_c$, so all spectral components are close to the corresponding FSR harmonics. At this set of frequencies, the modulation transfer function (15) gives $H_M(k\Omega_m) \simeq \pm 1/jk\Delta\Omega\tau_c$, and so it acts as an integrator with time constant

$\Delta\tau = \pm\Delta\Omega_m\tau_c/\Omega_m$. The modal phase function is thus determined by the equation

$$\Delta\tau \frac{d\Phi}{dt} = \varphi(t) \tag{21}$$

The modes of the FM laser (19) are recovered from (21) for $\varphi(t) = \mu\cos(\Omega_m t + \theta)$, and are generalized in this regime to arbitrary periodic functions. As in regime 1, the instantaneous modal frequency follows the imparted phase $\varphi(t)$, but the frequency excursion now entails a factor $1/\Delta\tau$, which represents an enhancement by $\Omega_m/\Delta\Omega_m$ with respect to regime 1. For arbitrary periodic PM waveforms, this regime was identified in [47] and more recently exploited in [30] for signal generation applications.

• If the spectral content of the applied phase function $\varphi(t)$ is located near semi-integer values of the FSR, $(1/2+k)\omega_c$ with k integer, the transfer function is approximately flat with $H_\mathrm{M}(\Omega_m) \simeq 1/2$ and the modal phase function is halved with respect to the applied phase. This regime is depicted as region 3 in Fig. 2.

2.2. Frequency-shifting cavities

In FS cavities, the field undergoes a frequency shift $\exp(j\varphi(t)) = \exp(j\Omega_s t)$ in each recirculation, where Ω_s is the shifting frequency. The solution to (7) is a linearly chirped function:

$$\Phi(t) = \frac{\Omega_s}{2\tau_c} t(t+\tau_c) \tag{22}$$

According to the equivalent representation of Fig. 1(b), the FS cavity can be understood as an unmodulated ring resonator preceded and followed by complementary chirp modulations or time lenses. In this regard, signal processors employing chirp modulation followed by a resonator and direct detection such as those in [50, 51] are functionally similar to FS cavities. The modal content of the FS cavity can be described as

$$E_m(t) = e^{j\frac{\Omega_s}{2\tau_c}t^2 + j\frac{\Omega_s}{2}t} \sum_k A_k e^{jk\omega_c t} \tag{23}$$

namely, as a set of linearly chirped functions carried by evenly spaced in frequency.

When the cavity is operated above threshold, (23) constitutes the basis of the moving comb model of the laser emission. According to this model, the output is continuously driven by spontaneous emission, which is regeneratively amplified in the spectral net gain region while it is shifted in frequency in multiple recirculations. In this process, the chirped mode is selected from ASE by the filtering properties of the cavity. The amplification ceases when the chirped mode exits the gain region and the mode becomes below threshold. This results in a representation similar to (23) but with the constant amplitudes A_k substituted by envelopes $A_k(t)$ slowly varying at the roundtrip time scale and with a duration equal to the transit time in the spectral net gain region [37–39].

3. Experimental setup and results

3.1. Modes of a PM fiber loop

A first experiment was designed to provide direct evidence in a PM fiber loop of the modal decomposition (12), the modulation transfer function (15), and the equivalent model in Fig. 1(b). The experimental setup is shown in Fig. 3. The fiber loop (FSR = 6.903 MHz) is shown in red, and includes a phase modulator (V_π = 4.7 V) driven by an arbitrary waveform generator (AWG1), a PZT fiber stretcher (Idil Fibres Optiques) for active stabilization, filter couplers for power injection and extraction, an isolator to ensure unidirectional recirculation, a home-made

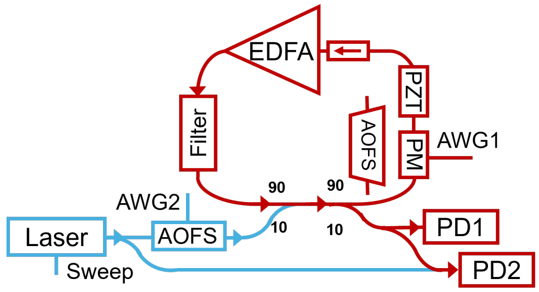

Fig. 3. Experimental setup.

EDFA consisting of 60 cm of highly-doped fiber (Liekki Er80/8) pumped at 980 nm and offering up to ~ 19 dB of gain and a noise figure < 3.5 dB, and a flat-top tunable filter (EXFO XTM-50) centered at 1550 nm to prevent the loop from lasing at 1532 nm. The system was based on polarization-maintaining components, except the EDFA. A polarization controller, not shown in the figure, was placed before the filter to adjust the recirculating state of polarization. Active stabilization for CW injection was provided by an error signal measured after tapping the loop's output and measuring the intensity at photodiode PD1 followed by electrical lowpass filtering.

Additional elements for signal injection and analysis are also shown in blue in the figure. A tunable single-wavelength fiber laser at ~ 1550 nm with a linewidth < 100 Hz (NKT Koheras E15) is used for injection and heterodyne measurement of the loop's output. The injected field is engineered through a fiber-coupled acousto-optics frequency shifter (AOFS) (AA Opto) controlled through a second arbitrary waveform generator (AWG2). The AOFS allows for implementing both frequency upshift and frequency modulation and sinusoidal phase modulation in the 80 ± 5 MHz range through the driving waveform. The heterodyne measurements were carried out by a 40-GHz photodiode (PD2) followed by a 6-GHz real time oscilloscope (LeCroy SDA 6000A). For intensity measurements, a low bandwidth photodiode followed by a 5-MHz digitizer (Digilent) is used. In our third experiment, the intracavity PM was substituted by the AOFS, as is shown in the figure. The loop's output power ranges between −16 dBm and −13 dBm, depending on the concrete experiment.

With the loop operating below threshold, the seed wavelength was scanned using a ramp signal spanning ~ 65 MHz at a frequency of 120 Hz. Switching transients, however, reduce the linear sweep range to an excursion of ~ 56 MHz with a quasi-static sweep rate $\gamma = 8.093$ kHz/µs, sufficient to clearly scan 7 cavity resonances. In Fig. 4(a) we depict the output intensity of the unmodulated loop when neither the internal nor the external PM are applied, in a range where three consecutive spectral resonances are swept. They present a low finesse $\mathcal{F} = 13$ corresponding to a single-pass roundtrip amplitude decay factor $\rho = 0.782$, as is inferred from the fit in Fig. 4(d).

We analyzed the loop's output intensity in different situations of internal (intraloop) PM and with externally injected PM fields engineered through the AOFS. Fig. 4(b) shows the effect of an internal sinusoidal PM $\exp(j\varphi(t))$ with modulation index $\mu = 1$ rad and modulation frequency $f_m = \Omega_m/2\pi = 300$ kHz, in the absence of external PM. In this instance, the resonance shows amplitude modulation (AM) at two distinct frequencies: f_m on the resonance's slopes and $2f_m$ at the center. This phenomenon is evident in the high-resolution trace of Fig. 5(a). This trace can be straightforwardly analyzed from the equivalent model of Fig. 1(b). There, the unmodulated cavity acts on a PM wave with sinusoidal modulation $\exp(-j\Phi(t))$ and index $\beta = 3.674$ rad, as given by (17). As intensity measurements are insensitive to the output PM in Fig. 1(b), the depicted trace can be interpreted as the effect of a discriminator on a swept PM wave, with a high phase-to-amplitude conversion to the fundamental f_m at the resonance's slopes and a lower

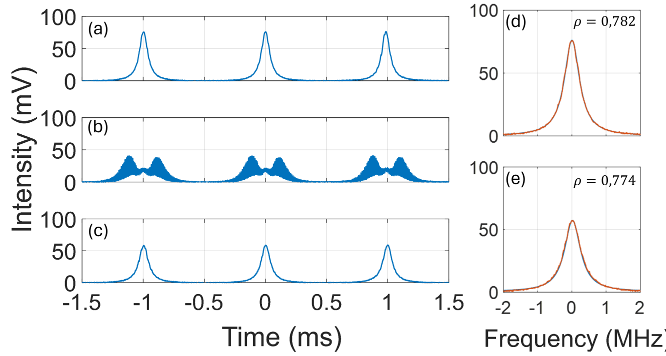

Fig. 4. Wavelength sweep with (a) internal and external (AOFS) sinusoidal phase modulations off, (b) internal on and external off, and (c) internal on and external on after fine tuning the delay. (d) and (e), zoom of a single resonance (blue) and fitted shape (orange) when (d) both internal and external phase modulations are off and (e) both are on. The difference in the traces is barely perceptible.

conversion to the second harmonic $2f_m$ at the resonance's peak.

Afterwards, the input wavelength was phase modulated in the AOFS by $\exp(j\Phi(t))$ to compensate for the input modulation $\exp(-j\Phi(t))$ in the equivalent model, and so let the swept wavelength pass through an unmodulated loop. The AOFS driving waveform was then fine tuned in delay, a procedure that synchronizes the compensating PM $\exp(j\Phi(t))$ and the internal phase modulation. The result is shown in Fig. 4(c), where the PM-AM conversion ripples are now absent and the resonances of an unmodulated resonator, zoomed in (e), recovered.

According to (12), this compensation means that we have seeded the PM loop with one of its optical modes, which therefore passes through the resonator unaltered up to a constant. To check this view, we switched off the wavelength sweep and fixed it at 1550 nm, providing active stabilization of the cavity at this wavelength. Then, we connected the heterodyne path in Fig. 3 and retrieved the heterodyne spectrum of the output, shown in Fig. 5(b) with a blue trace. Comparison with the corresponding spectrum of the externally engineered compensating input field (orange trace) shows the coincidence of both. The spectra appear centered at 80 MHz due to the frequency shift imparted by the AOFS, which allows for the direct visualization of the double-sided PM spectra and so to extract the modulation index β by fitting the spectral lines to the Bessel functions $J_k^2(\beta)$ ($k = 0, \pm 1, \pm 2, \dots$). This yields a value $\beta = 3.622$ again in agreement with the theory. This result not only evidences the excitation of the PM cavity mode, but also confirms the presence of the PM factor $\exp(j\Phi(t))$ at the output of the equivalent model of Fig. 1(b). Finally, we extracted the modulation transfer function $H_M(\Omega_m)$ as the ratio of modal β and intraloop μ modulation indices for different values of f_m. The comparison of the experimental values (dots) and the modulation transfer function is shown in Fig. 5(c). Notably, this procedure allows for the validation of (17) within the complete first FSR and in a range of relative modulation indices spanning more than two orders of magnitude, surpassing the value obtained in previous studies of DFB FM lasers [52] and integrated PM resonators [48].

The final part of this experiment aimed at illustrating the injection of non-sinusoidal PM modes. We employed a square signal as intraloop PM $\varphi(t)$ with $f_m = 20$ kHz and peak phase values $\pm\mu = \pm 0.278$ rad. This signal in entirely contained in region 1 of Fig. 2, and so the instantaneous frequency of the modal phase function $\Phi(t)$, as given by (20), switches $\pm\mu/2\pi\tau_c = \pm 305$ kHz above and below the swept carrier. This binary FM mode can be externally injected using the AOFS as a frequency modulator, with a driving frequency that switches between these two

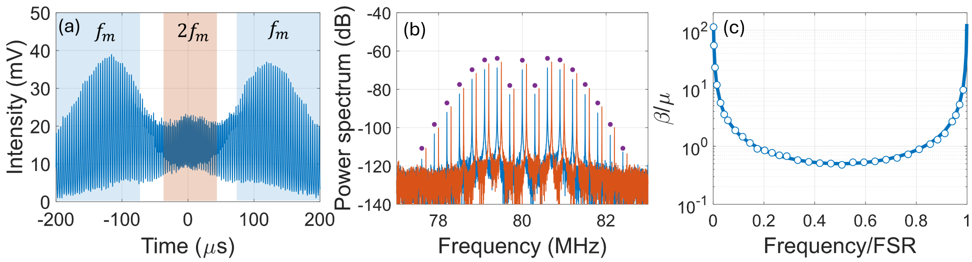

Fig. 5. (a) High-resolution trace of a resonance in Fig. 4(b). (b) Optical heterodyne spectra of (blue) the loop's output, (orange) the 1550-nm input wavelength phase modulated in the AOFS, and (purple dots) fitted values of the Bessel functions. The orange trace is upshifted by 100 kHz to ease the comparison. (c) PM transfer function: experimental (dots) and theory (blue trace).

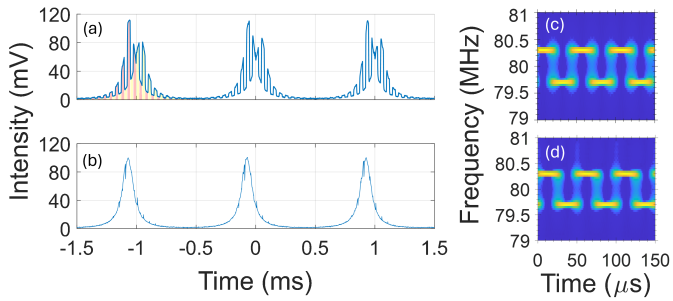

Fig. 6. (a) Intensity of a wavelength sweep with internal square phase modulation on and external (AOFS) modulation off. Red and yellow bands are included in the first peak to help visualize the two interleaved resonaces. (b) Intensity of a wavelength sweep with both internal and external square frequency modulations, after fine tuning the delay. (c) and (d), spectrograms of the heterodyne signal of (c) the loop's output and (d) the 1550-nm input wavelength frequency modulated in the AOFS.

frequencies above and below 80 MHz. In Fig. 6(a) we show the output intensity observed when only the internal PM is activated. According to the equivalent model of Fig. 1(b), this trace can be interpreted as the transit through an unmodulated cavity of two time-interleaved wavelength-swept carriers separated by ±305 kHz, resulting in the observed pair of time-interleaved resonances. If the AOFS is now turned on and the delay of the frequency switching tuned, we recover the initial resonances as is shown in Fig. 6(b). The glitches appearing in the otherwise smooth trace are due to the AOFS switching time. Under these conditions, but now with the wavelength fixed and the loop stabilized, we retrieved the optical field's spectrogram from the heterodyne signal to compare the injected seed, measured after the AOFS and shown in Fig. 6(c), with the loop's output field, depicted in Fig. 6(d). In both cases we observe the same ±305 kHz frequency excursion. The coincidence of these spectrograms shows again the injection of a cavity mode, here in the form of two switched frequencies.

3.2. FM laser modes

A second set of experiments were aimed at exploring the FM laser emission modes and its relationship with the PM cavity modes. We refer loosely here as a FM laser to any non-modelocked emission of a PM active cavity above threshold, although strictly speaking FM laser were originally driven by sinusoidally PM with modulation frequency near the FSR or one of

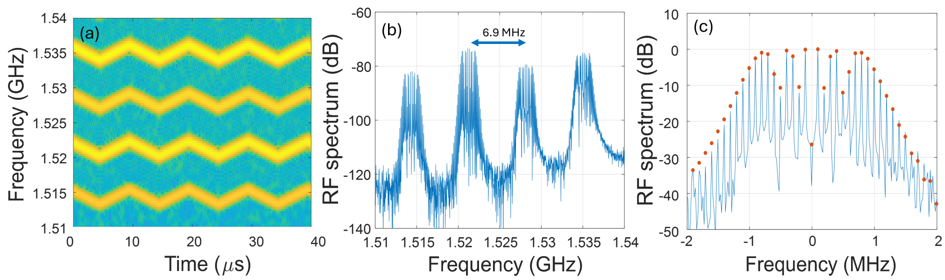

Fig. 7. Narrowband multimode FM laser emission. (a) Spectrogram of the heterodyne signal when the local oscillator was placed ~ 1.5 GHz below the FM laser emission peak. (b) Spectrum of the heterodyne signal, showing the multiple modal spectra separated by an FSR. (c) Comparison of (blue) the normalized modal spectrum of the triangular FM laser mode centered at 1.522 GHz and (orange dots) the spectrum predicted by the theory (triangular frequency modulation with $f_m = 100$ kHz and excursion ± 1.1 MHz).

its harmonics. A first demonstration was targeted to show a narrowband multimode FM laser emission. With the fiber loop pumped above threshold, the internal PM $\varphi(t)$ was configured as a triangular wave with peak phase excursion $\pm\mu = \pm 1$ rad at a repetition rate $f_m = 100$ kHz. From the point of view of cavity modes, this waveform is contained in region 1 of Fig. 2 and therefore the modal phase function $\Phi(t)$ entails an instantaneous frequency that deviates $\pm\mu/2\pi\tau_c = \pm 1.10$ MHz from each axial mode of the unmodulated cavity. The FM laser emission was multimodal with significant mode competition, as expected due to the flat top character of the intracavity filter [31,46]. The spectrotemporal characteristics of the laser emission modes coincide with the PM cavity modes, as could be directly visualized through the spectrogram of the heterodyne signal shown in Fig. 7(a). Note the coincidence in phase of the frequency excursions in different modes, in agreement with (12). In Fig. 7(b) we show the optical spectrum as retrieved from the heterodyne signal. Here, the different groups of modal spectra, mutually separated by an FSR, are clearly discernible. The modal spectrum is zoomed and compared in Fig. 7(c) with the triangular phase-modulated modal spectrum of the corresponding PM cavity mode, with an excellent agreement.

We then addressed the generation of wideband singlemode emission with different internal phase modulation functions $\varphi(t)$ in regime 2 of Fig. 2. In this case, the tunable flat-top filter was substituted by a Gaussian apodized fiber Bragg grating (Technica) with Bragg wavelength 1550.24 nm and width 1.6 nm (FWHM) to favor singlemode emission. The PZT actuator was also removed from the loop. This resulted in an FSR that changed slightly to 7.760 MHz. We first introduced sinusoidal PM near the FSR and recovered the basic phenomenology already described in similar FM fiber lasers [47,53], in particular the induction of FM modelocking for deviations with respect to the FSR of up to a few kHz [53] and FM laser operation with spectral width of up to 6 GHz [47], in our case limited by the heterodyne detection bandwidth. Afterwards, we introduced a triangular phase modulation, now with a modulation frequency slightly deviated from the sixth FSR harmonic ($f_m = 46.600$ MHz) and with an excursion $\pm\mu = \pm 0.47$ rad. The observed laser emission was singlemode and followed a triangular excursion in instantaneous frequency, as shown in the heterodyne trace depicted in Fig. 8(a) and the spectrogram in Fig. 8(b). The first trace also evidences the presence of AM due to PM-AM conversion in the slopes of the intracavity Gaussian filter [42]. The heterodyne optical spectrum, shown in Fig. 8(c), is then expected to be distorted as compared with the spectrum of a cavity mode with triangular instantaneous frequency and excursion $\pm(\mu/2\pi\tau_c)\,(f_m/\Delta f_m)$, as described by (21), since filtering

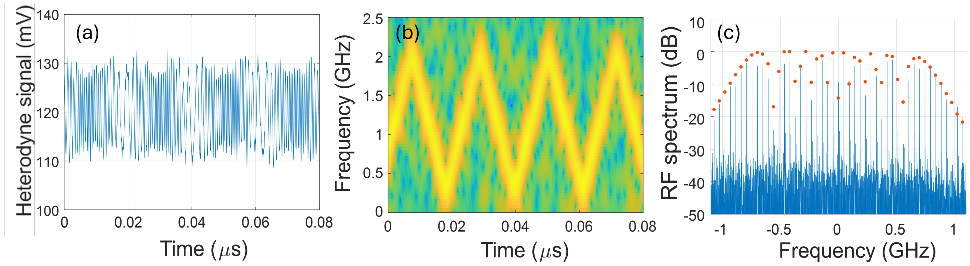

Fig. 8. Wideband singlemode FM laser emission. (a) Heterodyne signal when the local oscillator was placed ~ 1.2 GHz below the emission peak. (b) Spectrum of the heterodyne signal (blue) and spectrum of a triangular FM with $f_m = 46.600$ MHz and excursion ±894 MHz (orange dots). (c) Spectrogram of the heterodyne signal.

effects are not included in our theory. In this figure we also show with dots the result of the best fit of the experimental data with a spectrum of this form, where the overall agreement is good but not exact. The fitted excursion of ±894 MHz is indeed higher than the estimate provided by the theory, ±676 MHz.

We finally point out that, in general and in contrast with the optical spectrum, the spectrogram does not permit to elucidate the single or multimode character of the FM laser, as it is limited by the time-frequency resolution limit of spectral analysis. In the spectrogram, it is necessary to choose time bins of duration $\Delta t \ll 1/f_m$ to clearly resolve the internal structure of the instantaneous frequency within a modulation period, and we also need a spectral resolution $\Delta\nu < \mathrm{FSR} = 1/\tau_c$ to resolve adjacent axial modes. As both scales are related by $\Delta t \Delta\nu \sim 1$, it is thus necessary that $f_m \tau_c \ll 1$, and this limits the use of the spectrogram as a complete modal characterization tool to the regime 1 of Fig. 2. A similar problem limits the detection of the chirped modes of FSF lasers by spectral analysis to the regime of small frequency shifts, defined by the condition $f_s \tau_c < 1$ where $f_s = \Omega_s/2\pi$ is the shifting frequency [36, 39].

3.3. FSF laser modes

In final experiment, we validated the model (23) of CW FSF laser emission. We substituted the internal phase modulator in Fig. 3 by the AOFS, driven by at shifting frequency $f_s = 80$ MHz. The FSR changed to a value of 8.426 MHz and the peak of the CW FSF emission showed at 1550.07 nm. In this configuration, the laser is similar to that used in our previous study [54]. The local oscillator was tuned to the emission peak and the heterodyne signal, plotted in Fig. 9(a), recorded. As expected, the spectrogram did not show any clear evidence of decomposition (23) since the laser operated in the regime of large frequency shifts $f_s \tau_c \simeq 9.5$. To detect the modal structure, we numerically constructed a complex representation of the optical field by removing the dc component of the heterodyne signal and performing a Hilbert transform to get the quadrature component. Then, we conducted a blind search of chirp components by a digital cross-correlation of the optical field with linearly chirped test functions $E_\gamma(t) = \exp\left(j\pi\gamma t^2\right)$ of variable rate γ. The result is shown in Fig. 9(b), where the presence of chirped functions only at the expected rate $\gamma = f_s/\tau_c = 674$ MHz/µs is apparent. According to (23), the result of the cross-correlation for this chirp rate should be:

$$R(u) = \int dt E_\gamma(t + u/2)^* E_m(t - u/2) \quad = \frac{\tau_c}{f_s} \sum_k (-1)^k A_k \delta(u - k/f_s) \tag{24}$$

comprising a set of amplitudes A_k evenly spaced in the temporal lag variable u with separation $1/f_s$. This structure is clearly visible in the experimental cross-correlation depicted in Fig. 9(c).

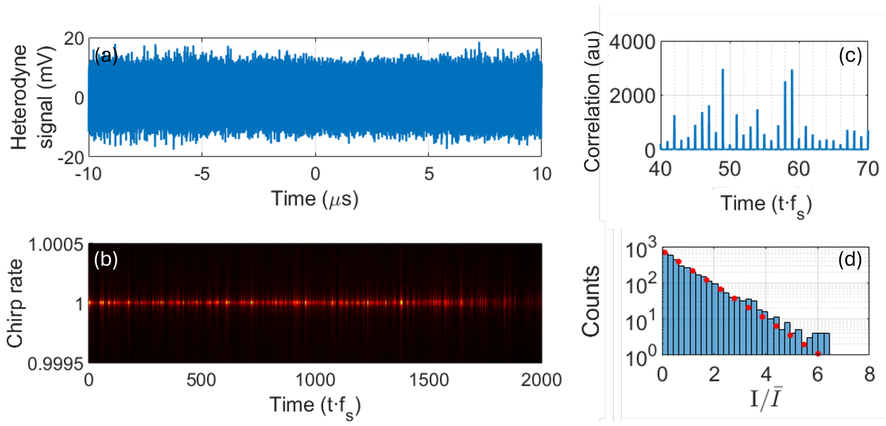

Fig. 9. CW FSF laser emission. (a) DC-subtracted heterodyne signal. (b) Color map of the cross-correlation of the heterodyne signal and linear chirp functions of variable chirp rate γ, in relative units $\gamma\tau_c/f_s$. (c) Zoom of the cross correlation with a linear chirped function with rate $\gamma = f_s/\tau_c$. (d) Distribution histogram of random intensities and, with red dots, best fit to a negative exponential function $\exp(-sI_k/\overline{I})$, with $s = 1.090$.

From this trace, a statistical test of the modal structure was devised after noticing that the random amplitudes A_k, which are polarized in the present setup, are created by spontaneous emission events. The distribution of the intensities $I_k = |A_k|^2$ relative to the mean $\overline{I}$ should therefore be negative exponential $\exp(-I_k/\overline{I})$ [55], in agreement with the experiment as shown in Fig. 9(d).

It is remarkable that a linear theory (23) is so neatly reflected in the CW FSF laser output, as this indicates that nonlinear dynamical effects are, if not absent, not relevant. The first point here is that the saturation dynamics is determined by the gain's recovery time, which is of the order of ms in an Er:fiber laser [54]. This time scale is large compared with the roundtrip time, which is sub-µs. Therefore, the regeneratively amplified, frequency-shifted recirculation of ASE that generates the chirped modes is a linear process that follows adiabatically the gain dynamics. Moreover, in the experiment, the local oscillator in the heterodyne interferometer was placed at the emission peak, where gain equals loss [40] and the chirps flow with almost constant amplitudes A_k, as described by (23). This result represents the first, to the best of our knowledge, direct validation of the moving comb model in the regime of large frequency shifts, as the original study focused on the complementary region [36]. We finally mention that hybrid modes implemented as an intracavity combination of frequency shift and sinusoidal phase modulation have been demonstrated in [45].

4. Conclusion

We have presented a linear operator theory that accounts of the response of dispersionless PM and FS cavities or resonators under arbitrary optical inputs and modulation profiles. The PM/FS cavity has been described as a filter that selects a certain class of fields, invariant under multiple roundtrips, which have been identified with the PM/FS cavity modes. The optical modes have been shown to correspond to the axial modes of the unmodulated ring cavity, phase modulated by the solution of the linear equation (7) with minimum spectral width. This approach extends in a consistent way the modal concept to PM/FS cavities and resonators, and leads to a system's level equivalence, and thus independent of the technology, of PM/FS cavities or resonators with resonators preceded and followed by modal phase modulations.

The theory has been experimentally validated through the external injection of sinusoidal PM and binary FM modes in an Er:fiber PM fiber loop. The cavity modes have also been compared with the emission modes in a FM and a FSF Er:fiber laser, showing the effects of finite gain bandwidth and mode competition in the FM laser and the chirped structure of the FSF laser emission. In the analysis, the limitations of the spectrogram as a characterization tool in the regime of large phase modulation frequency or frequency shift have been identified. These results provide a unified view of the modal structure of cavities and resonators incorporating phase modulation and/or frequency shift as well as general tools for its linear analysis of interest in the fields of photonic signal generation and processing.

Funding. Agencia Estatal de Investigación (PID2020-120404GB-I00, EQC2019-006189-P); Ministerio de Universidades (FPU21/05449).

Disclosures. The authors declare no conflicts of interest.

Data Availability Statement. Data underlying the results presented in this paper are not publicly available at this time but may be obtained from the authors upon reasonable request.

References

1. K.-P. Ho and J. M. Kahn, "Optical frequency comb generator using phase modulation in amplified circulating loop," IEEE Photonics Technol. Lett. **5**, 721–725 (1993).
2. S. Bennett, B. Cai, E. Burr, *et al.*, "1.8-THz bandwidth, zero-frequency error, tunable optical comb generator for DWDM applications," IEEE Photonics Technol. Lett. **11**, 551–553 (1999).
3. T. Kawanishi, T. Sakamoto, S. Shinada, and M. Izutsu, "Optical frequency comb generator using optical fiber loops with single-sideband modulation," IEICE Electron. Express **1**, 217–221 (2004).
4. P. Shen, N. J. Gomes, P. A. Davies, *et al.*, "Analysis and demonstration of a fast tunable fiber-ring-based optical frequency comb generator," J. Light. Technol. **25**, 3257–3264 (2007).
5. M. Kourogi, K. Nakagawa, and M. Ohtsu, "Wide-span optical frequency comb generator for accurate optical frequency difference measurement," IEEE J. Quantum Electron. **29**, 2693–2701 (1993).
6. L. R. Brothers, D. Lee, and N. C. Wong, "Terahertz optical frequency comb generation and phase locking of an optical parametric oscillator at 665 GHz," Opt. Lett. **19**, 245–247 (1994).
7. T. Saitoh, M. Kourogi, and M. Ohtsu, "A waveguide-type optical-frequency comb generator," IEEE photonics technology letters **7**, 197–199 (1995).
8. P. Sekhar, C. Fredrick, D. R. Carlson, *et al.*, "20 GHz fiber-integrated femtosecond pulse and supercontinuum generation with a resonant electro-optic frequency comb," APL Photonics **8**, 116111 (2023).
9. A. Kaplan, A. Greenblatt, G. Harston, *et al.*, "Tunable frequency comb generator based on $LiNbO_3$ ring resonator," in *Optical Amplifiers and Their Applications/Coherent Optical Technologies and Applications,* (Optica Publishing Group, 2006), p. CFC3.
10. N. Dupuis, C. R. Doerr, L. Zhang, *et al.*, "InP-based comb generator for optical OFDM," J. Light. Technol. **30**, 466–472 (2011).
11. I. Demirtzioglou, C. Lacava, K. R. Bottrill, *et al.*, "Frequency comb generation in a silicon ring resonator modulator," Opt. Express **26**, 790–796 (2018).
12. M. Zhang, B. Buscaino, C. Wang, *et al.*, "Broadband electro-optic frequency comb generation in a lithium niobate microring resonator," Nature **568**, 373–377 (2019).
13. Y. Hu, M. Yu, B. Buscaino, *et al.*, "High-efficiency and broadband on-chip electro-optic frequency comb generators," Nat. Photonics **16**, 679–685 (2022).
14. E. J. Tough, M. J. Fice, G. Carpintero, *et al.*, "InP integrated optical frequency comb generator using an amplified recirculating loop," Opt. Express **30**, 43195–43208 (2022).
15. T. Zhang, K. Yin, C. Zhang, *et al.*, "Integrated electro-optic frequency combs: Theory and current progress," Laser & Photonics Rev. **18**, 2301363 (2024).
16. B. Fischer, B. Vodonos, S. Atkins, and A. Bekker, "Experimental demonstration of localization in the frequency domain of mode-locked lasers with dispersion," Opt. Lett. **27**, 1061–1063 (2002).
17. S. Longhi, "Dynamic localization and Bloch oscillations in the spectrum of a frequency mode-locked laser," Opt. letters **30**, 786–788 (2005).
18. C. Bersch, G. Onishchukov, and U. Peschel, "Spectral and temporal Bloch oscillations in optical fibres," Appl. Phys. B **104**, 495–501 (2011).
19. L. Yuan and S. Fan, "Bloch oscillation and unidirectional translation of frequency in a dynamically modulated ring resonator," Optica **3**, 1014–1018 (2016).
20. L. Yuan, Q. Lin, M. Xiao, and S. Fan, "Synthetic dimension in photonics," Optica **5**, 1396–1405 (2018).
21. A. Dutt, M. Minkov, Q. Lin, *et al.*, "Experimental band structure spectroscopy along a synthetic dimension," Nat. Commun. **10**, 3122 (2019).
22. Y. Hu, C. Reimer, A. Shams-Ansari, *et al.*, "Realization of high-dimensional frequency crystals in electro-optic microcombs," Optica **7**, 1189–1194 (2020).

23. N. Englebert, N. Goldman, M. Erkintalo, *et al.*, "Bloch oscillations of coherently driven dissipative solitons in a synthetic dimension," Nat. Phys. **19**, 1014–1021 (2023).
24. V. Durán, H. Guillet de Chatellus, C. Schnebélin, *et al.*, "Optical frequency combs generated by acousto-optic frequency-shifting loops," IEEE Photonics Technol. Lett. **31**, 1878–1881 (2019).
25. H. Yang, M. Brunel, M. Vallet, *et al.*, "Analysis of frequency-shifting loops in integer and fractional Talbot conditions: electro-optic versus acousto-optic modulation," J. Opt. Soc. Am. B **37**, 3162–3169 (2020).
26. H. Yang, L. Wang, C. Zhao, and H. Zhang, "Sinusoidal frequency-modulated waveforms generated by a phase-modulated frequency-shifting loop," J. Light. Technol. **39**, 3112–3120 (2021).
27. H. Yang, M. Brunel, M. Vallet, *et al.*, "Optical frequency-to-time mapping using a phase-modulated frequency-shifting loop," Opt. Lett. **46**, 2336–2339 (2021).
28. M. Brunel, L. Frein, A. Carré, *et al.*, "Nonlinear frequency chirps from a stabilized injected phase-modulated fiber laser loop," in *EPJ Web of Conferences,* vol. 287 (EDP Sciences, 2023), p. 07015.
29. W. Lyu, H. Tian, Z. Fu, *et al.*, "Pulse generation with programmable positions based on a phase-modulated optical frequency-shifting loop," Opt. Lett. **48**, 3411–3414 (2023).
30. W. Lyu, H. Tian, Z. Fu, *et al.*, "Broadband microwave signal generation with programmable chirp shapes via low-speed electronics-controlled phase-modulated optical loop," Opt. Express **33**, 2542–2557 (2025).
31. S. Harris and O. McDuff, "Theory of FM laser oscillation," IEEE J. Quantum Electron. **1**, 245–262 (1965).
32. A. E. Siegman, *Lasers* (University Science Books, 1986).
33. D. Taylor, S. Harris, S. Nieh, and T. Hansch, "Electronic tuning of a dye laser using the acousto-optic filter," Appl. Phys. Lett. **19**, 269–271 (1971).
34. F. V. Kowalski, P. D. Hale, and S. J. Shattil, "Broadband continuous-wave laser," Opt. Lett. **13**, 622–624 (1988).
35. W. Streifer and J. R. Whinnery, "Analysis of a dye laser tuned by acousto-optic filter," Appl. Phys. Lett. **17**, 335–337 (1970).
36. S. Balle, I. C. M. Littler, K. Bergmann, and F. V. Kowalski, "Frequency shifted feedback dye laser operating at a small shift frequency," Opt. Commun. **102**, 166–174 (1993).
37. K. Nakamura, F. Abe, K. Kasahara, *et al.*, "Spectral characteristics of an all solid-state frequency-shifted feedback laser," IEEE J. Quantum Electron. **33**, 103–111 (1997).
38. L. P. Yatsenko, B. W. Shore, and K. Bergmann, "Theory of a frequency-shifted feedback laser," Opt. Commun. **236**, 183–202 (2004).
39. H. Guillet de Chatellus, E. Lacot, W. Glastre, *et al.*, "The hypothesis of the moving comb in frequency shifted feedback lasers," Opt. Commun. **284**, 4965–4970 (2011).
40. H. Sabert and E. Brinkmeyer, "Pulse generation in fiber lasers with frequency shifted feedback," J. Light. Technol. **12**, 1360–1368 (1994).
41. J.-N. Maran, P. Besnard, and S. LaRochelle, "Theoretical analysis of a pulsed regime observed with a frequency-shifted-feedback fiber laser," J. Opt. Soc. Am. B **23**, 1302–1311 (2006).
42. S. Longhi and P. Laporta, "Time-domain analysis of frequency modulation laser oscillation," Appl. Phys. Lett. **73**, 720–722 (1998).
43. Y. Li, S. M. Goldwasser, P. R. Herczfeld, and L. Narducci, "Dynamics of an electrooptically tunable microchip laser," IEEE J. Quantum Electron. **42**, 208–217 (2006).
44. S. Longhi and P. Laporta, "Floquet theory of intracavity laser frequency modulation," Phys. Rev. A **60**, 4016 (1999).
45. M. Cuenca, H. Maestre, and C. R. Fernández-Pousa, "Modes of frequency-modulated and frequency-shifted feedback lasers," in *2024 International Topical Meeting on Microwave Photonics (MWP),* (2024), pp. 1–4.
46. S. E. Harris and B. Buscaino, "Technique for generating broadband FM light," Opt. Lett. **45**, 2058–2061 (2020).
47. S. L. Girard, H. Chen, G. W. Schinn, and M. Piché, "Frequency-modulated, tunable, semiconductor-optical-amplifier-based fiber ring laser for linewidth and line shape control," Opt. Lett. **33**, 1920–1922 (2008).
48. Z. Wan, Q. Cen, Y. Ding, *et al.*, "Virtual-state model for analyzing electro-optical modulation in ring resonators," Phys. Rev. Lett. **132**, 123802 (2024).
49. A. Siegman and D. Kuizenga, "Active mode-coupling phenomena in pulsed and continuous lasers," Opto-electronics **6**, 43–66 (1974).
50. J. Li, S. Fu, X. Xie, *et al.*, "Low-latency short-time Fourier transform of microwave photonics processing," J. Light. Technol. **41**, 6149–6156 (2023).
51. X. Xie, J. Li, K. Xu, *et al.*, "Broadband linear frequency modulation signal compression based on a spectral Talbot effect," Opt. Lett. **48**, 5383–5386 (2023).
52. A. Lucero, R. Tkach, and R. Derosier, "Distortion of the frequency modulation spectra of semiconductor lasers by weak optical feedback," Electron. Lett. **24**, 337–339 (1988).
53. K. S. Abedin, N. Onodera, and M. Hyodo, "Widely-chirped high-repetition-rate continuous wave FM laser oscillation in Erbium fiber ring laser," Jpn. J. Appl. Phys. **37**, L649 (1998).
54. M. Cuenca, H. Maestre, G. Torregrosa, *et al.*, "ASE recirculation effects in pulsed frequency shifted feedback lasers at large frequency shifts," Opt. Express **31**, 15615–15636 (2023).
55. J. W. Goodman, *Statistical Optics* (John Wiley & Sons, 2015).

Appendix. Modulation with resonant components

Solutions to (7) when the phase function $\varphi(t)$ contains resonant components, namely, periodic components with period equal to the roundtrip time τ_c, can be obtained using the following result. Given a solution $\Phi_\theta(t)$ of (7) obtained from an input phase function $\varphi_\theta(t)$ that depends on a continuous parameter θ, this solution gives rise to a family of solutions $\Phi_{\alpha(t)}(t)$ corresponding to $\varphi_{\alpha(t)}(t)$ where the parameter is substituted by a function $\alpha(t)$ periodic in the roundtrip time, $\alpha(t) = \alpha(t+\tau_c)$. Explicitly,

$$\Phi_{\alpha(t-\tau_c)}(t-\tau_c) + \varphi_{\alpha(t)}(t) = \Phi_{\alpha(t)}(t-\tau_c) + \varphi_{\alpha(t)}(t) = \Phi_{\alpha(t)}(t) \tag{25}$$

where the first equality follows from the assumed periodicity of $\alpha(t)$ and the second because $\Phi_\theta(t)$ is a solution of (7) with $\varphi_\theta(t)$ for any value of θ. In words, a resonant function can substitute for any parameter in a given solution of (7).

Let us use this property to determine the solution for resonant modulations, where $\varphi(t)$ is itself periodic with period τ_c. To this end, consider that we introduce in the optical cavity a constant, wavelength independent, phase $\varphi(t) = \theta$. This type of phases appear, for instance, as the Fresnel reflection phase in mirrors incorporated in a laser ring cavity, and simply shift in frequency the position of resonances defined by the ring resonator. The corresponding modal solution to (7) is $\Phi(t) = \theta t/\tau_c$. If we apply the previous property to this situation, the solution corresponding to a resonant modulation $\varphi(t) = \alpha(t)$ is given by:

$$\Phi(t) = \alpha(t)\frac{t}{\tau_c} \tag{26}$$

as is immediate to check. As an application example, we compute the intracavity field for resonant modulation when the seed field is monochromatic, $E_s(t) = E_0 e^{j\omega_0 t}$. In this case, the Neumann series (3) can be summed since T commutes with $e^{j\varphi(t)}$, and yields [1,25]:

$$E_c(t) = E_0 \sum_{n=0}^{\infty} \rho^n e^{jn\alpha(t)+jn\omega_0 t} = \frac{E_0}{1-\rho\, e^{j\omega_0 t + j\alpha(t)}} \tag{27}$$

The same expression is obtained using (26) in (8) due to the unitary equivalence $e^{j\Phi(t)}Te^{-j\Phi(t)} = e^{i\varphi(t)}T$.

As said, the result can be applied to any parameter in a known solution, therefore introducing resonant components in the corresponding mode. Consider, for instance, sinusoidal PM and suppose that we provide a resonant modulation to the driving phase, $\varphi(t) = \mu\cos(\Omega_m t + \alpha(t))$. The modal phase function then writes:

$$\Phi(t) = \beta\sin(\Omega_m(t+\tau_c/2) + \alpha(t)) \tag{28}$$

thus describing the same mode but incorporating the applied resonant modulation in the phase. Another example is provided by the amplitude of any driving waveform since, if $\Phi(t)$ is a solution of (7) for given $\varphi(t)$, so is $\mu\Phi(t)$ for $\mu\varphi(t)$ with μ an arbitrary constant. Then, the above derived property indicates that the modal phase function for a drive of the form $\widetilde{\varphi}(t) = \alpha(t)\varphi(t)$ with $\alpha(t) = \alpha(t+\tau_c)$ periodic, is $\widetilde{\Phi}(t) = \alpha(t)\Phi(t)$.